AIP Applied Physics Letters

Identifying and characterizing epitaxial graphene domains on partially graphitized SiC(0001) surfaces using scanning probe microscopy

Joshua A. Kellar, Justice M. P. Alaboson, Qing Hua Wang, and Mark C. Hersam

Citation: Appl. Phys. Lett. **96**, 143103 (2010); doi: 10.1063/1.3378684
View online: http://dx.doi.org/10.1063/1.3378684
View Table of Contents: http://apl.aip.org/resource/1/APPLAB/v96/i14
Published by the American Institute of Physics.

Additional information on Appl. Phys. Lett.

Journal Homepage: http://apl.aip.org/
Journal Information: http://apl.aip.org/about/about_the_journal
Top downloads: http://apl.aip.org/features/most_downloaded
Information for Authors: http://apl.aip.org/authors

ADVERTISEMENT

Downloaded 01 Oct 2012 to 18.189.35.30. Redistribution subject to AIP license or copyright; see http://apl.aip.org/about/rights_and_permissions

Identifying and characterizing epitaxial graphene domains on partially graphitized SiC(0001) surfaces using scanning probe microscopy

Joshua A. Kellar,[1] Justice M. P. Alaboson,[1] Qing Hua Wang,[1] and Mark C. Hersam[1,2,a)]
[1]*Department of Materials Science and Engineering, Northwestern University, Evanston, Illinois 60208, USA*
[2]*Department of Chemistry, Northwestern University, Evanston, Illinois 60208, USA*

(Received 20 January 2010; accepted 30 January 2010; published online 5 April 2010)

Scanning tunneling microscopy (STM), atomic force microscopy (AFM), lateral force microscopy (LFM), and conductive AFM (cAFM) are employed to characterize epitaxial graphene on SiC(0001). Of particular interest are substrates that possess single-layer and bilayer graphene domains, which form during thermal decomposition of silicon from SiC(0001). Since these samples are often partially graphitized, characterization techniques are needed that can distinguish domains of epitaxial graphene from the adjacent $(6\sqrt{3}\times6\sqrt{3})R30°$ reconstructed SiC(0001) surface. The relative merits of STM, AFM, LFM, and cAFM for this purpose are outlined, thus providing nanometer-scale strategies for identifying and characterizing epitaxial graphene. © *2010 American Institute of Physics*. [doi:10.1063/1.3378684]

Graphene, a two-dimensional honeycomb lattice of carbon atoms, has been intensely studied in recent years due its unique electronic, mechanical, and chemical properties.[1–3] Among the many strategies for preparing graphene,[4] epitaxial graphene grown on silicon carbide surfaces shows significant promise for realizing graphene-based electronics. For example, it is compatible with traditional device fabrication techniques, and the electronic properties of the silicon carbide substrate can be independently tuned from insulating to conductive via doping.[5–8] To realize properties that show the most promise for device applications, single-layer graphene (SLG) and bilayer graphene (BLG) are desirable, which are formed during the early stages of thermal decomposition of silicon from the SiC(0001) surface. However, since these substrates do not necessarily possess a fully graphitized surface, subsequent characterization is required to determine the level of graphitization and to distinguish domains of epitaxial graphene from the adjacent carbon-rich $(6\sqrt{3}\times6\sqrt{3})R30°$ reconstructed SiC(0001) surface.

In this letter, we present a scanning probe microscopy (SPM) investigation of partially graphitized SiC(0001). While atomic-scale spatially resolved structural information is provided by ultrahigh vacuum (UHV) scanning tunneling microscopy (STM), this relatively specialized technique is not routinely integrated with conventional fabrication techniques. On the other hand, ambient atomic force microscopy (AFM) techniques, such as lateral force microscopy (LFM) and conductive AFM (cAFM), provide a straightforward means of spatially mapping frictional and electronic properties with nanometer-scale spatial resolution. While crosstalk between frictional and topographic signals complicates LFM analysis, cAFM unambiguously distinguishes graphene from the exposed $(6\sqrt{3}\times6\sqrt{3})R30°$ reconstructed SiC(0001) surface. Overall, this letter outlines the relative merits of STM, AFM, LFM, and cAFM for identifying and characterizing epitaxial graphene domains on partially graphitized SiC(0001).

A schematic of a partially graphitized SiC(0001) substrate is shown in Fig. 1(a). The first carbon-rich layer is not a true graphene structure but instead an interface layer that is partially covalently bound to the bulk silicon carbide. This layer possesses a $(6\sqrt{3}\times6\sqrt{3})R30°$ reconstruction as determined by low energy electron diffraction and STM.[9,10] Subsequent graphene layers that develop on top of the $(6\sqrt{3}\times6\sqrt{3})R30°$ interface layer (referred to as $6\sqrt{3}$ for short) during thermal decomposition of silicon are weakly coupled to the substrate and can continuously cover the underlying SiC steps.[11–13] Since growth conditions that yield SLG and/or BLG domains often lead to incomplete surface graphitization, exposed regions of $6\sqrt{3}$ can also be present on these substrates.

In this study, partially graphitized SiC(0001) samples were prepared in a home-built UHV system[14] operated at a

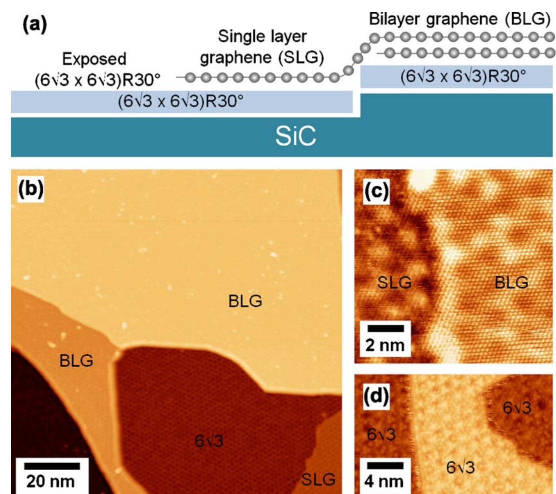

FIG. 1. (Color online) (a) Cross-sectional schematic diagram of a partially graphitized SiC(0001) surface. (b) UHV STM image of a partially graphitized SiC(0001) surface with regions of single-layer graphene (SLG), bilayer graphene (BLG), and exposed $6\sqrt{3}$ reconstruction indicated. Imaging conditions: −2.0 V sample bias, 0.05 nA tunneling current. (c) Atomically resolved image of SLG and BLG. Imaging conditions: −0.4 V sample bias, 0.1 nA tunneling current. (d) Atomically resolved image of an exposed $6\sqrt{3}$ region. Imaging conditions: −2.0 V sample bias, 0.1 nA tunneling current.

a)Electronic mail: m-hersam@northwestern.edu.

 © 2010 American Institute of Physics

Downloaded 01 Oct 2012 to 18.189.35.30. Redistribution subject to AIP license or copyright; see http://apl.aip.org/about/rights_and_permissions

base pressure of 5×10^{-11} Torr. The 6H-SiC(0001) n-type substrates (Cree, Inc.) were degreased by ultrasonication in acetone and isopropanol before being outgassed in the UHV chamber overnight at 600 °C by resistive heating. The samples were then annealed at 1100 °C to remove the surface oxide layer and form the $6\sqrt{3}$ interface layer. The surface was graphitized by annealing the substrate at 1350 °C for several cycles of 30 s, producing primarily SLG along with smaller regions of BLG and exposed $6\sqrt{3}$ reconstruction. The surface was imaged using the same UHV system. Topographic STM scans were conducted at room temperature in constant-current mode with the bias voltage applied to the sample. The STM tips were electrochemically etched W or commercially available PtIr (Agilent Technologies).

All AFM images were collected utilizing a modified CP Research (Thermomicroscopes) AFM. Current mapping of the graphitized SiC surface was achieved with a Pt-coated probe (μMasch, NSC36C). Imaging was performed in contact mode with an applied force of ~10 nN, fast scan speed of 0.3 μm/s, and sample bias of +0.3 V. Current was collected through the cAFM probe using a current preamplifier (DL Instruments, Model 1212) and a 160 Hz low-pass in-line filter. A limiting resistor (~12 MΩ) was used in series with the preamplifier to limit the current and thus maximize cAFM probe lifetime. The cAFM probes were tested on Au and highly ordered pyrolytic graphite reference samples, and contact resistances of <5 kΩ were recorded before imaging. Contact mode topography and LFM signals were collected concurrently with the current signal. Intermittent contact mode topography imaging also utilized the same multipurpose cantilevers. AFM images were rendered using WSXM SPM analysis software.[15]

Representative UHV STM images of the partially graphitized SiC(0001) surface are shown in Figs. 1(b)–1(d). As observed in Fig. 1(b), the surface is mainly SLG along with some portions of BLG and exposed $6\sqrt{3}$ reconstruction. Similar to previous reports,[10,11] the corrugation of the $6\sqrt{3}$ regions is clearly visible. SLG appears smoother than the exposed $6\sqrt{3}$, but the $6\sqrt{3}$ periodicity is still visible through the graphene layer, and the BLG is smoother still. At lower sample bias, it is possible to resolve the carbon lattice of the graphene layers, as shown in Fig. 1(c). The single layer graphene region appears as a hexagonal lattice, whereas the BLG region appears as a triangular lattice due to AB stacking between layers. A high resolution image of the $6\sqrt{3}$ region is also shown in Fig. 1(d), revealing a characteristic structure of clusters as reported previously.[9,10] STM imaging in several regions of the surface established a typical graphene terrace width of 50–200 nm, and exposed $6\sqrt{3}$ region widths of 10–100 nm. Overall, UHV STM enables unambiguous identification of SLG and BLG domains from exposed $6\sqrt{3}$ regions, albeit with limited throughput and nontrivial integration with conventional fabrication schemes.

In contrast to UHV STM, AFM techniques can be efficiently employed in ambient conditions, which enables more rapid and convenient characterization before, during, or after sample processing and device fabrication. Figure 2 shows a series of images of the same region of a partially graphitized SiC(0001) surface using a variety of AFM techniques. Figures 2(a) and 2(b) are contact mode AFM topography images where the fast scan direction is left-to-right and right-to-left, respectively, while Figs. 2(c) and 2(d) are LFM images that were taken concurrently with the contact mode AFM topography images. The LFM images show strong contrast with islands of increased friction compared to the remainder of the surface. The islands of increased friction have a typical size in the 10–100 nm regime, which agrees with the exposed $6\sqrt{3}$ region size measured with UHV STM. The assignment of the islands of increased friction to exposed $6\sqrt{3}$ is also consistent with previous UHV AFM studies that found significantly higher friction on SiC compared to epitaxial graphene.[16] However, this strong frictional contrast leads to an inversion in the contact mode AFM topography between left-to-right and right-to-left scans as seen in Figs. 2(a) and 2(b), which indicates significant crosstalk between the LFM and topography signals.[17] While measures can be taken to minimize this effect and consequently gather more accurate frictional and topography data in contact mode,[18] it is desirable to identify more straightforward means for circumventing this complication. For example, Fig. 2(e) contains an intermittent contact mode AFM image, where accurate topographical information is directly measured.

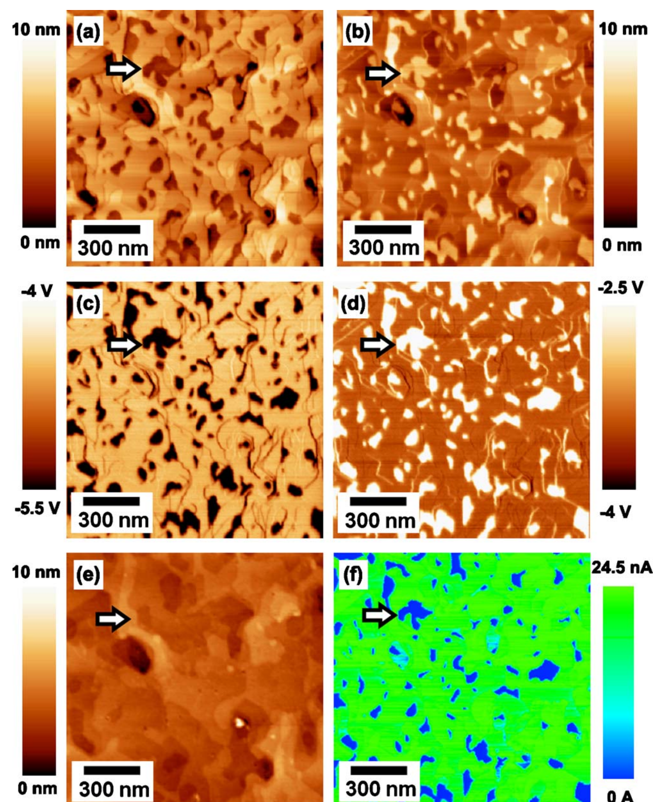

FIG. 2. (Color online) [(a) and (b)] Contact-mode AFM topography images of a partially graphitized SiC(0001) surface with fast scan direction of (a) left-to-right and (b) right-to-left. Note the height inversion of the exposed $6\sqrt{3}$ domains due to topography-LFM crosstalk (see arrow). [(c) and (d)] LFM images with fast scan direction of (c) left-to-right and (d) right-to-left, showing high frictional contrast between the graphene and exposed $6\sqrt{3}$ regions. (e) Intermittent contact mode AFM topography and (f) contact mode cAFM image (+0.3 V sample bias) of the same region.

While intermittent contact mode AFM enables rapid and reliable topographical imaging of partially graphitized SiC(0001) substrates, it does not provide clear contrast between exposed $6\sqrt{3}$ regions and epitaxial graphene domains. On the other hand, by directly monitoring the electrical current through the AFM tip during contact mode imaging, cAFM can spatially map local electrical properties.[19] Figure 2(f) contains a cAFM image of the same region imaged in

Downloaded 01 Oct 2012 to 18.189.35.30. Redistribution subject to AIP license or copyright; see http://apl.aip.org/about/rights_and_permissions

Figs. 2(a)–2(e). Strong cAFM contrast is observed with significantly less current detected on the $6\sqrt{3}$ regions compared to the epitaxial graphene domains. The cAFM contrast results from an increased tip-sample contact resistance on the $6\sqrt{3}$ regions compared to epitaxial graphene, which can likely be attributed to the increased electrical conductivity and/or decreased oxidation susceptibility of graphene compared to silicon carbide. While the maximum current in Fig. 2(f) is intentionally limited with a series resistor to prevent prolonged exposure of the cAFM tip to high current densities, currents on the order of microamperes (i.e., resistance $<100\ \mathrm{k}\Omega$) are observed on the epitaxial domains when the limited resistor is removed. Since the current detected in the exposed $6\sqrt{3}$ regions is in the subnanoampere regime (i.e., resistance $>1\ \mathrm{G}\Omega$), rapid and unambiguous spatial mapping of epitaxial graphene domains compared to exposed $6\sqrt{3}$ regions is readily achieved with cAFM imaging.

In conclusion, partially graphitized SiC(0001) surfaces have been characterized with a suite of scanning probe techniques. UHV STM provides atomic-scale spatial resolution and can distinguish regions of single-layer and bilayer epitaxial graphene from adjacent exposed $6\sqrt{3}$ domains but is relatively laborious and is not easily integrated with typical device fabrication steps. On the other hand, AFM can be performed in ambient conditions, enabling efficient characterization with nanometer-scale spatial resolution. LFM reveals strong frictional contrast between epitaxial graphene domains and exposed $6\sqrt{3}$ regions but crosstalk between LFM and topographic signals complicates quantitative analysis. Finally, cAFM takes advantage of strong tip-sample contact resistance differences to provide the highest imaging contrast between epitaxial graphene and exposed $6\sqrt{3}$. By delineating the relative merits of STM, AFM, LFM, and cAFM, this study is likely to guide future efforts to identify, characterize, and utilize epitaxial graphene in fundamental studies and device applications.

This work was supported by the National Science Foundation (Award Nos. EEC-0647560 and DMR-0520513), the Office of Naval Research (Award No. N00014-09-1-0180), and Argonne National Laboratory (ANL). ANL is a U.S. Department of Energy Office of Science Laboratory operated under Contract No. DE-AC02-06CH11357 by UChicago Argonne, LLC. The authors also thank Joseph Lyding for use of his STM control software.

[1]K. S. Novoselov, A. K. Geim, S. V. Morozov, D. Jiang, M. I. Katsnelson, I. V. Grigorieva, S. V. Dubonos, and A. A. Firsov, Nature (London) **438**, 197 (2005).
[2]A. K. Geim and K. S. Novoselov, Nature Mater. **6**, 183 (2007).
[3]A. K. Geim, Science **324**, 1530 (2009).
[4]A. A. Green and M. C. Hersam, J. Phys. Chem. Lett. **1**, 544 (2010).
[5]C. Berger, Z. M. Song, X. B. Li, X. S. Wu, N. Brown, C. Naud, D. Mayou, T. B. Li, J. Hass, A. N. Marchenkov, E. H. Conrad, P. N. First, and W. A. de Heer, Science **312**, 1191 (2006).
[6]W. A. de Heer, C. Berger, X. S. Wu, P. N. First, E. H. Conrad, X. B. Li, T. B. Li, M. Sprinkle, J. Hass, M. L. Sadowski, M. Potemski, and G. Martinez, Solid State Commun. **143**, 92 (2007).
[7]G. Gu, S. Nie, R. M. Feenstra, R. P. Devaty, W. J. Choyke, W. K. Chan, and M. G. Kane, Appl. Phys. Lett. **90**, 253507 (2007).
[8]Luxmi, P. J. Fisher, N. Srivastava, R. M. Feenstra, Y. Sun, J.Kedzierski, P. Healey, and G. Gu, Appl. Phys. Lett. **95**, 073101 (2009).
[9]C. Riedl, U. Starke, J. Bernhardt, M. Franke, and K. Heinz, Phys. Rev. B **76**, 245406 (2007).
[10]G. M. Rutter, N. P. Guisinger, J. N. Crain, E. A. A. Jarvis, M. D. Stiles, T. Li, P. N. First, and J. A. Stroscio, Phys. Rev. B **76**, 235416 (2007).
[11]P. Lauffer, K. V. Emtsev, R. Graupner, T. Seyller, L. Ley, S. A. Reshanov, and H. B. Weber, Phys. Rev. B **77**, 155426 (2008).
[12]T. Seyller, K. V. Emtsev, K. Gao, F. Speck, L. Ley, A. Tadich, L. Broekman, J. D. Riley, R. C. G. Leckey, O. Rader, A. Varykhalov, and A. M. Shikin, Surf. Sci. **600**, 3906 (2006).
[13]Q. H. Wang and M. C. Hersam, Nat. Chem. **1**, 206 (2009).
[14]E. T. Foley, N. L. Yoder, N. P. Guisinger, and M. C. Hersam, Rev. Sci. Instrum. **75**, 5280 (2004).
[15]I. Horcas, R. Fernandez, J. M. Gomez-Rodriguez, J. Colchero, J. Gomez-Herrero, and A. M. Baro, Rev. Sci. Instrum. **78**, 013705 (2007).
[16]T. Filleter, J. L. McChesney, A. Bostwick, E. Rotenberg, K. V. Emtsev, T. Seyller, K. Horn, and R. Bennewitz, Phys. Rev. Lett. **102**, 086102 (2009).
[17]R. Piner and R. S. Ruoff, Rev. Sci. Instrum. **73**, 3392 (2002).
[18]M. W. Such, D. E. Kramer, and M. C. Hersam, Ultramicroscopy **99**, 189 (2004).
[19]M. C. Hersam, A. C. F. Hoole, S. J. O'Shea, and M. E. Welland, Appl. Phys. Lett. **72**, 915 (1998).

Downloaded 01 Oct 2012 to 18.189.35.30. Redistribution subject to AIP license or copyright; see http://apl.aip.org/about/rights_and_permissions